Electronic Structure, Molecular Interaction, and Stability of the CH_4-nH_2O Complex, for $n = 1-21$

Graciela Bravo-Pérez,* Armando Cruz-Torres, and Ascención Romero-Martínez

Programa de Ingeniería Molecular, Instituto Mexicano del Petróleo, Eje Central Lázaro Cárdenas 152, 07730 México D. F., Mexico

Received: November 5, 2007; Revised Manuscript Received: July 4, 2008

Molecular calculations were carried out with four different methodologies to study the CH_4-nH_2O complex, for $n = 1-21$. The HF and MP2 methods used considered the O atom with pseudopotential to freeze the $1s^2$ shell. The other methodologies applied the Bhandhlyp and B3lyp exchange and correlation functionals. The optimized CH_4-nH_2O structures are reported, specifying the number and type of H_2O subunits (triangle, square, pentagon, etc.) that comprised the nH_2O counterpart cluster or cage, that interacted with the CH_4 molecule, and, in the latter case, that provided its confinement. Results are focused to understand the stability of the CH_4-nH_2O complex. The quality of the electron correlation effect, as well as the size of the nH_2O cage to confine the guest molecule, and the number and type of H_2O subunits comprising the nH_2O cluster or cage are the most important factors to provide the stability of the complex and also dictate the particular n value at which the CH_4 molecule confinement occurs. This number was 14 for the HF, Bhandhlyp, and B3Lyp methods and 16 for the MP2 method. The reported hydrate structures for $n < 20$ could be predictive for future experiments.

1. Introduction

Hydrocarbon hydrates are inclusion compounds formed by H_2O molecules in crystalline arrangements that are stabilized by the presence of small hydrocarbon molecules. Their investigation is of great importance to deal with different industrial problems. The microscopic understanding of its formation and stabilization is related to current and new energetic and industrial concerns.[1,2] For the industry of oil extraction, the formation of hydrates represents an unavoidable problem for natural gas production, transportation, and processing. At temperatures near water freezing and pressures above 40 bar, methane hydrates normally agglomerate, causing blockages in the hydrocarbon transport pipeline. These conditions are obtained in deep-water offshore fields.[3] For several decades, hydrate formation studies were focused on this problem.[4] It is now well-known that the hydrate structure has a direct relation with the deepness in the location of the sea floor extraction.[5] Low-weighted hydrocarbon hydrates are also matters for investigations to find an alternative to natural gas storage and transportation.[6] Another interest is the CH_4 extraction from its hydrated form to count for a larger source number of this conventional fuel.[7] Another matter of study is the selective separation of a hydrocarbon mixture.[8−10] The environmental concern is also related to hydrate formation studies;[11−13] sequestration of the CO_2 molecule, once hydrated, by the substitution of a hydrocarbon molecule[14] is one of the topics.[15]

In this paper we carried out molecular calculations of the CH_4-nH_2O ($n = 1-21$) complex to determine the optimum structures and the interaction of the nH_2O counterpart structure with the CH_4 molecule. We focused on the particular n value for which the encapsulation of the CH_4 molecule succeeded and on the main microscopic features relevant for this to occur. Experiments and simulation studies have clearly identified the smallest H_2O cage able to encapsulate the CH_4 molecule as a basic "building block" cavity formed with 12 faces of 5 sides per face, given the abbreviation 5^{12}. From this form different hydrate crystal structures, that is, I (small, 5^{12}; large, $5^{12}6^2$), II (small, 5^{12}; large, $5^{12}6^4$), and H (small, 5^{12}; medium, $4^35^66^3$; large, $5^{12}6^8$), can be generated.[5,16] Our results show that CH_4 molecule confinement may happen already from water cages with a smaller number of H_2O molecules than $n = 20$. We expect to provide with this work some contribution to the future investigation of hydrate formation and its inhibition.

2. Computational Details

The geometries of the CH_4-nH_2O ($n = 1-21$) complex were optimized with the following methods: HF/cep-4 g, MP2/cep-4 g, BHandHLYP/6-311 g(d,p), and B3LYP/6-311 g(d,p), that will be denoted in the text as the HF, MP2, BH&H, and B3LYP methods, respectively. The first two made use of the atomic pseudopotential of Krauss et al.[17] for the O atom, freezing the $1s^2$ shell and treating the valence electrons with a minimum basis set. Two polarization functions, *d* to O and *p* to H atoms, were explicitly added, with coefficients equal to 1. These coefficients were tested with the H_2O molecule and H_2O dimer, providing very good agreements in the geometry and dipole moment (DM) values, relative to the experiments[18−20] (see Table 1). Only recently, the exchange and correlation B3LYP functional and the second-order Møller−Plesset approximation have been used in molecular optimizations of hydrated molecules.[21−24] These methods provide good results for the intra- and intermolecular interactions. The BH&H functional was more commonly used to describe molecules of the gas environmental reactivity, with cases of an H atom abstraction represented in the metastable state. This transition-state structure may include nonbonded atom pairs or molecule subunits that interact between each other through very small pair−particle forces,[25−27] similar to the guest molecule−water cage interactions that we studied in this work. Therefore, calculations with the BH&H method were included,

* Corresponding author. E-mail: gbperez@imp.mx. Phone: (+5255) 9175 6410. Fax: (+5255) 9175 6380.

10.1021/jp7106268 CCC: $40.75
Published on Web 08/20/2008

TABLE 1: H_2O, $(H_2O)_2$, and CH_4 Calculation Parameters: Interatomic Distance (Ångstroms), Angle (Degrees), D_e (Kilocalories per Mole), DM (Debye), and First Lowest Frequency Eigenvalue (per Centimeter)

CH_4			
method	CH	HCH	freq eigenvalue
HF	1.121	109.47	1432, →
MP2	1.130	109.47−109.48	1363, →
BH&H	1.082	109.45−109.49	1389, →
B3LYP	1.090	109.34−109.57	1340, →
expt[30]	1.100	109.50	

H_2O				
method	OH	HOH	DM	freq eigenvalue
HF	0.980	104.40	1.99	1682, →
MP2	1.003	100.80	2.06	1638, →
BH&H	0.954	104.68	2.11	1743, →
B3LYP	0.963	103.81	2.07	1723, →
expt	0.953−0.971[29]	104.50−108.41[19,29,52,53]	1.85−3.09[29,54]	

$(H_2O)_2$					
method	O−O	OHO	D_e	DM	freq eigenvalue
HF	3.132	179.54	3.29	2.88	102, →
MP2	2.851	173.06	4.67	2.48	114, →
BH&H	2.872	173.60	7.53	2.80	93, →
B3LYP	2.910	165.25	7.62	2.17	23, →
expt	2.65−2.98[18,19,28,55,56]	161.16−177.70[18,19,28]	4.85−5.44[18,20]	2.11−2.60[19,29]	

TABLE 2: Binding Energy (Kilocalories per Mole) Including the ZPE Correction for the CH_4 and H_2O Molecules

	HF	MP2	BH&H	B3LYP	expt[a]
$CH_4 \rightarrow 4H + C$	344.47091	391.56187	384.47736	391.88190	397.5
$H_2O \rightarrow OH + H$	83.491161	106.60084	106.67551	111.62651	119.0

[a] Reference 57.

also to be compared with the other methods. The H_2O molecule and H_2O dimer were also calculated with the BH&H and B3LYP methods and provided a good agreement with the experiment, although for the dimer, location of a local minimum was very difficult, and the fact is reflected with the very small frequency eigenvalue obtained (see Table 1). The methods that best described the electron correlation effect showed the best agreement with the experiment.[19,28,29] The parameters of the CH_4 molecule are also included in Table 1.[30] In Table 2 are reported the binding energies of the H_2O and CH_4 molecules, relative to their atomic and OH dissociation products. As in Table 1, the methods with the better electron correlation effect are closer to the experiment. The ZPE correction contributed a 7−9% improvement for the CH_4 molecule and a 7−10% improvement for the H_2O molecule.

The chosen methodology to calculate the CH_4-nH_2O (n = 1−21) complex should be sensitive enough to reproduce the H bond in a H_2O network[18,31,32] as well as the even smaller London dispersion interactions of it with the CH_4 molecule. The methodology should also not be very demanding in computation requirement, in order to have access to large n values. Fortunately, the four methods we applied could reproduce the H bond in the H_2O clusters and the guest$-nH_2O$ interactions in a very reasonable way, as is discussed in the following sections.

The geometries encapsulating the CH_4 molecule were searched from the very small sizes. For this purpose, the starting geometries had always the CH_4 molecule surrounded by n H_2O molecules homogeneously distributed at distances large enough (∼3.5 Å) from it to avoid any chemical interaction between the CH_4 molecule and the H_2O network. The geometry optimizations were carried out without symmetry restrictions. The optimized geometries of a less robust method, in terms of computation requirement, were normally inputs for more sophisticated methods. The MP2 optimizations were taken from optimum geometries of the HF method as well as the trials for the B3LYP method were optimum structures from the BH&H method. The final geometries, except for the case of the MP2 method in the range n = 14−21, were considered with frequency calculations at the same level of approximation to be confirmed as local minima. Only local minimum structures and the MP2 structures of the n = 14−21 range are reported. The calculations were carried out using the Gaussian 98 program.[33]

3. Results and Discussion

3.1. Structures for the n = 1−8 Range. The optimized geometries of the $CH_4-(1-8)H_2O$ complex are shown in Figure 1, and the geometry parameters for the n = 2−8 sizes are reported in Table 3a for the HF and BH&H methods (in the Supporting Information) and Table 3b for the MP2 and B3LYP methods. The n = 1 complex is reported in Table 4. O−O refers to the averaged O−O distance of each structure, O−H is the averaged nearest distance between H and O, OHO is the averaged angle formed by the two nearest O atoms and the H atom that forms an H bond, and C−O is the shortest C to O distance.

Let us first analyze the n = 1 complex. This is a very difficult interaction because it is mainly due to London dispersion forces and the electron correlation effect that the different methods provided in different degrees, participating less than in the larger (n > 1) sizes. We believe that an increase in the electron correlation effect, caused by the increase in the nH_2O counterpart structure, facilitated, for the larger CH_4-nH_2O systems, the location of local minima. For the optimization of the n = 1

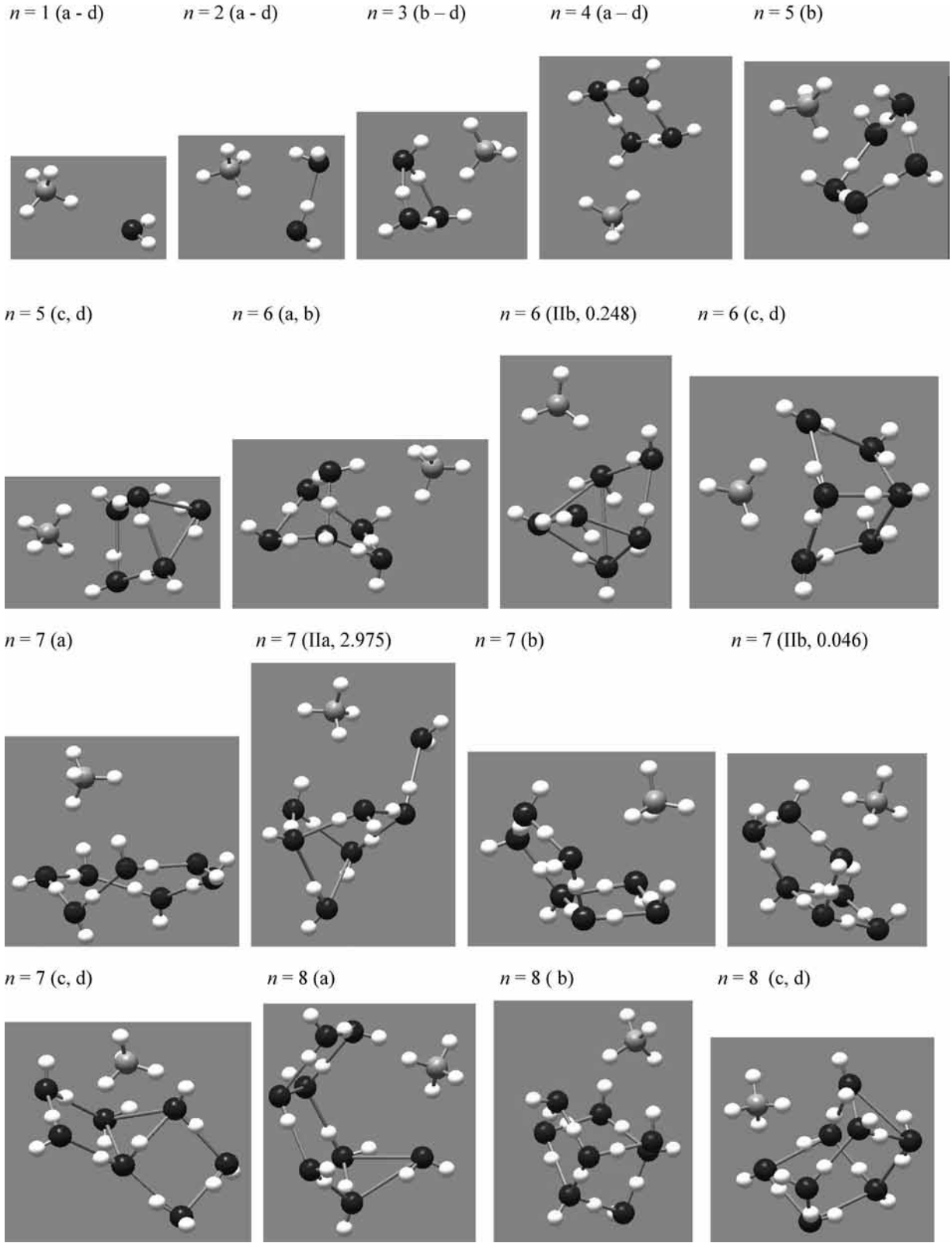

Figure 1. Optimized geometries for the $CH_4-(1-8)H_2O$ complex. The HF (a), MP2 (b), BH&H (c), and B3LYP (d) methods were considered. The geometry parameters are reported in Tables 3a (in the Supporting Information) and 3b. Within parentheses is indicated the isomer number that is shown (I, II, III, etc.), the applied method, and its energy difference, kilocalories per mole, relative to isomer I.

complex, we first started with trial geometries of a random orientation of the CH_4 molecule relative to the H_2O molecule, but we could not converge to a local minimum except for the MP2 method, which anyway accounted for an extremely flat potential surface. Then, we tried with the other methods to start with trial geometries taken from the once optimized $n = 2$ complex, and extracting one H_2O molecule, also refining some convergence parameters. In this way we achieved also local minima for these methods. The frequency modes that accounted for the C−O intermolecular oscillation were, in fact, very low, ranging between 45 and 57 cm^{-1} for the HF and MP2 methods and between 106 and 114 cm^{-1} for the BH&H and B3LYP

TABLE 3B: Geometrical Parameters for the $CH_4-(1-8)H_2O$ Complex (Ångstroms, Degrees)

	MP2				B3LYP			
n	OO	OH	OHO	CO	OO	OH	OHO	CO
2	2.831	1.011	169.0	3.651	2.880	0.960	166.2	3.492
3	2.602	1.030	156.1	3.740	2.770	0.971	151.3	3.551
4	2.530	1.072	172.3	3.730	2.722	0.982	165.0	3.500
5	2.510	1.070	176.2	3.782	2.781	0.980	157.1	3.562
6	2.533	1.053	170.2	3.763	2.740	0.981	163.2	3.443
7	2.500	1.092	175.2	3.710	2.740	0.982	161.0	3.574
8	2.481	1.100	172.0	3.713	2.771	0.981	166.4	3.532

methods (see Table 4). The orientation of the CH_4 molecule relative to the H_2O molecule, despite having a DM several orders of magnitude smaller than the DM of the water molecule,[34] could contribute with a dipole ↔ dipole interaction. To follow the CH_4 ↔ H_2O interaction for a broader range than the region of local minimum, we extended the C−O distance over a larger range, from 3 to 10 Å, without changing the rest of the geometry of the local minimum. The resulting curves may be seen in Figure 2S of the Supporting Information. By using a notation similar to soft-sphere type interactions, we estimate in Table 4 the size of the H_2O and CH_4 molecules, σ, and the well depth, ε, taking the intermolecular separation limit (C−O) at 10 Å from the calculation. The ε value was compared with the infinity separation limit of isolated CH_4 and H_2O molecules, and the largest errors occurred for the BH&H and B3LYP methods, which were lower than 4%. These curves represent an estimation of the CH_4 ↔ H_2O London interaction forces and are shown to be sensible for all methods, even for the HF method, which lacks the electron correlation effect. We will come back to ε and σ values later, when we discuss the stability of the CH_4-nH_2O complex ($n = 1-21$), in sections 3.5 and 3.6.

When a next H_2O molecule is included, then the CH_4 ↔ $2H_2O$ interaction, taking the MP2 values as examples, is 1.883 kcal/mol, which is about 4 times stronger than for the $n = 1$ complex. With regard to the electron charge distribution, the $n = 2$ complex accounted for a DM value of 2.10 Debye, which may be compared with the H_2O dimer reported in Table 1. It would be already expected that the approach of a nonpolar molecule, such as CH_4, to a H_2O network should alter the electron charge distribution of the latter. In our example case, the DM value of the H_2O dimer was lowered by 0.38 Debye.

With reference to Figure 1 again, more than one isomer was reported for the HF and MP2 methods. We discarded isomers with energies higher than 0.20 eV (or 4.612 kcal/mol) above that of isomer I, that is, the lowest energy isomer. Tables 3a and 3b (as well as Tables 5a,b and 6a,b, which include the parameters for the larger sizes and will be discussed in the following sections) include only parameters of isomer I. Exceptional cases will be explicitly noted. The optimum B3LYP structures were not modified from the BH&H forms; only slight differences were noted in the geometry parameters. However, between the HF and MP2 methods, various forms were observed in several cases. Basically, the triangular, square, pentagon, and hexagonal ring H_2O subunits, which are known stable H_2O clusters,[18,35−46] were also included as trial possibilities or combinations of them, even for the larger complexes. The complexes we report for the very small sizes ($n = 1-4$) agree in their nH_2O counterpart structure with the literature of water clusters as well as with studies of a van der Waals type interaction between a stable molecule and an nH_2O cluster.[47] The $n = 5$ and 6 sizes, for which a variety of planar and 3D water clusters were investigated in the literature to determine the 3D transition at $n = 6$, were also tested with our methods. For example, the prism, cage, and book forms of the $6H_2O$ cluster have been included as initial geometries. It is interesting that the HF and MP2 method final forms converged to an isomer composed by pentagon subunits, whereas for the BH&H and B3LYP methods, its first isomer denotes square subunits. This very incipient preference of the pentagon subunit for the MP2 method from these very small complexes will continue for larger sizes and will be thoroughly explained in section 3.4. The very low energy difference between isomers I and II of the MP2 method was also investigated by including the ZPE correction (for $T = 298$ K and 1 atm). With this correction the former isomers differed by 0.497 kcal/mol but remain in the same order. At $n = 7$ for the MP2 method we reported two isomers that belong to the same structure for which the main difference was the orientation of two of its H atoms that do not form H bonds. The relative orientation of these H atoms seemed to dictate the better stability of isomer I relative to isomer II. The energy difference by including the ZPE correction was 0.063 kcal/mol.

Concerning the HF method, one could note that the C−O and O−O distances were clearly relaxed relative to the other methods, affecting the final geometries, that showed, in some cases, atoms of a very low coordination number, or even unstable structures, as happened for the $n = 3$ and 5 cases. This is supported by the very low ε_{HF} value of Table 4, compared with the other methods. Also, note that the C−O distance from the other methods at the later sizes was larger than in the neighbor ($n = n \pm 1$) complex, corroborating the lower stability of the $n = 3$ and 5 complexes.[18,35,38] With the MP2 method, the O−O distance decreased inversely to n, which is a result earlier found by Xantheas[37] and explained by the increase in the electron correlation effect. With the BH&H and B3LYP methods the decrease was not so clearly identified. The MP2 O−O distance was shorter than with the BH&H and B3LYP methods and the C−O distance, larger. A better fitting from the MP2 method could be obtained by considering the coefficients of the added d and p polarization functions, or, in general, any additional functions to the basis set, to fit to the H_2O trimer, square, and or even pentagonal clusters, and not only for the water dimer, as we did. At the $n = 2 \rightarrow 3$ step, a remarkably higher contribution of the many body effect starts. Consequently, the $n = 3$ complex reported an O−O distance at most shortened relative to the $n = 2$ complex or H_2O dimer (see Table 1). The OH distance remained relatively constant for the HF, BH&H, and B3LYP methods; the latter two provided the best approach to the experimental value of water in the vapor phase.[19,31] With the MP2 method, the OH distance showed an incipient tendency to increase with n, as well as the OHO angle, to be almost aligned (near 180°). The MP2 method offered a very good description of the electron correlation, which influenced the results in different manners.

The square and pentagonal H_2O subunits started to show in the optimized structures of Figure 1. It will be shown in the following sections that these subunits kept showing for the larger sizes. The triangular subunit showed in few cases. This form was better favored with the BH&H and B3LYP methods (see the $n = 3$, 5, 7, and 8 cases). For the larger structures ($n > 8$) the cooperative H bond effect contributed more strongly so that the HF method could provide more compact structures.

3.2. Structures for the $n = 9-13$ Range. The optimized structures of the $CH_4-(9-13)H_2O$ complexes are shown in Figure 3, and the geometry parameters are reported in Table 5a for the HF and BH&H methods (found in the Supporting Information) and Table 5b for the MP2 and B3LYP methods.

TABLE 4: Parameters for the CH_4-H_2O Complex

method	C−O (Å)	OH (Å)[a]	OHC (deg)[b]	σ (Å)[c]	ε (kcal/mol)[d]	% error[e]	DM (Debye)	freq[f] (cm^{-1})
HF	4.051	0.990	174.21	3.64	0.3075	0.81	2.09	**45**, 51, 72, 87,...
MP2	3.822	1.000	178.50	3.40	0.4600	0.54	2.19	4.09. 14, 22, **57**,...
BH&H	3.554	0.952	167.91	3.12	2.2408	−3.60	2.02	20, **106**, 173, 196,...
B3LYP	3.580	0.971	170.42	3.09	2.7340	−1.37	1.90	**114**, 170, 177, 2.08,...

[a] Of the H_2O molecule. [b] That forms one H of the CH_4 molecule with O. [c] From the LJ type curve (see Figure 2S in the Supporting Information), taking the dissociating energy level from the calculation for C−O = 10 Å. For the HF and MP2 methods the calculation at C−O = 10 Å was lower in energy than the separated molecules, for the other methods, it was higher. [d] Dissociation energy, taken from the local minimum energy to the calculation at C−O = 10 Å. [e] Of the energy value reported in *d* relative to the value considering separated H_2O and CH_4 molecules. [f] Frequency eigenvalues. The number in bold is the eigenvalue of the C ↔ O oscillating mode.

For this size range it became clearer that the triangular subunit occurred more often with the BH&H and B3LYP methods. This happened for the whole $n = 9-13$ range, whereas with the HF method, it happened only for the second and fourth isomers of the $n = 9$ size and it did not happen at all with the MP2 method. The frequent presence of squares and pentagonal subunits was further confirmed. Rings of a larger size, such as a hexagon or a heptagon, started as well to be seen. It was also characteristic for this size range that the CH_4 approached the nH_2O cluster, producing a big hole in it, due to its stronger interaction with the nearest H_2O molecules, a kind of distorted ring subunit. In most cases this "ring" was in fact the largest hole in the nH_2O counterpart cluster and was always oriented facing the CH_4 molecule. This could be seen, for example, for the BH&H (B3LYP) method in the whole $n = 9-13$ range.

By comparison of the parameters between the BH&H and B3LYP methods, contractions in the O−H and C−O distance occurred with the former method. The consequent energy differences will be discussed in section 3.5. In general, the parameters behaved in this range very similar as for the $n = 6-8$ sizes. What most noticeably changed in the $n = 9-13$ sizes is the combination and number of the small subunits, that is, triangles, squares, pentagons, and hexagons, that were connected between each other to give rise to different nH_2O isomers. The C−O distance seemed to be more influenced by the structure of the nH_2O cluster itself. See, for example, the $n = 12$ case for the MP2 method. Isomer I reported a C−O distance of 3.70 Å, isomer II, a distance of 3.75, and isomer III, a distance of 3.69 Å, whereas the other parameters varied at most by 0.02 Å or 0°. The MP2 method showed the most compact forms for the $n = 10-13$ range. By "most compact", we mean structures with the largest number of very small subunits. At $n = 9$ the first isomer of the HF method was shown to be the most compact and is composed by a combination of squares and pentagons. At $n = 12$ the same first isomer is observed for the HF and MP2 methods, but the second and third isomers converged to different structures. The CH_4 molecule encapsulation did not happen for values of $n \leq 13$; therefore, it was necessary to increase the range.

3.3. Structures for the $n = 14-21$ Range and General Parameter Tendencies. The optimized geometries of the $CH_4-(14-21)H_2O$ complex are shown in Figure 4, and the geometry parameters are reported in Table 6a (in the Supporting Information) for the HF and BH&H methods and in Table 6b for the MP2 and B3LYP methods. At this *n* range the nH_2O counterpart clusters were more compact than in the $n = 9-13$ range and, in particular, the structures of the HF, BH&H, and B3LYP methods provided the most compact forms. They succeeded with the CH_4 molecule encapsulation, from the $n = 14$ size ($\equiv n_e$). By n_e we mean the smallest *n* value at which the nH_2O cluster could encapsulate the CH_4 molecule; this will be also referred to as the "first encapsulation size".

A particular very open nH_2O form of the MP2 method was obtained at $n = 16$ for isomer I. It is composed of pentagonal subunits and seems to be far from being able to encapsulate the CH_4 molecule. Interestingly, isomer II lies 1.614 kcal/mol above the former isomer and is composed with a very compact H_2O cage, encapsulating the CH_4 molecule. Then, for the MP2 method, $n_e = 16$. This second isomer with $n = 16$ is also a minimum in the C−O versus *n* curve that is shown in Figure 5. Then, isomer I of the MP2 method (geometry parameters: OO = 2.49 Å, OH = 1.09 Å, OHO = 177°, CO = 3.58 Å) was not considered in Table 6b or in Figures 5−13; instead, isomer II was taken. We also confirmed the energy ordering of isomers I and II by including the ZPE correction at normal conditions ($T = 298$ K, $P = 1$ atm). We calculated the ZPE correction at the HF and B3LYP levels of approximation, and for both cases the energy ordering was not modified, resulting in a HF correction energy difference of 9.310 kcal/mol and a B3LYP correction energy difference of 7.883 kcal/mol. This is one of the few cases where an nH_2O structure with a higher number of H bonds (21 for isomer II) is higher in energy than isomer I, which presents 16 H bonds. A structural difference between both isomers is the confinement or not of the CH_4 molecule. The stability of the CH_4-nH_2O complex relative to geometry parameters and confinement of the CH_4 molecule will be thoroughly discussed in sections 3.5 and 3.6. Also notice that the second isomer of the MP2 method had the same water cage as the water cage of the HF complex, composed of three squares, six pentagons, and one hexagon. Another similar situation occurred for $n = 14$. There, the type and number of subunits that took part in the $14H_2O$ cage, for all methods, was the same, that is, four squares, four pentagons, and one hexagon. The shorter O−O distances of the MP2 method produced a cage of smaller volume that could not confine the guest molecule. Because of the more relaxed O−O distance of the HF method, it produced water cages of the largest volume and the BH&H (B3LYP) method produced intermediate-sized cages.

For the $n = 20$ case, the dodecahedral (5^{12}) structure known in the literature was also considered in this study, with the BH&H and B3LYP methods. For this structure we obtained an average C−O distance of 3.772 Å for both methods, with minimum, maximum, and standard deviation values of 3.453, 4.220, and 0.233 Å, respectively, and for isomer I, we calculated an average C−O distance of 3.757 Å, with corresponding homologous values: 3.200, 4.58, and 0.548 Å. The structure 5^{12} calculated with the B3LYP method lies 27.9 kcal/mol above isomer I. Isomer I provided more available volume to the CH_4 molecule and also accounts for five more H bonds. These two properties favored isomer I at the most stable. In sections 3.5 and 3.6 we present a more detailed discussion of the role of the available volume to provide stability to the complex.

The geometry parameters of Tables 3, 5, and 6 are drawn versus *n* in Figures 5−7. At encapsulation, some of these

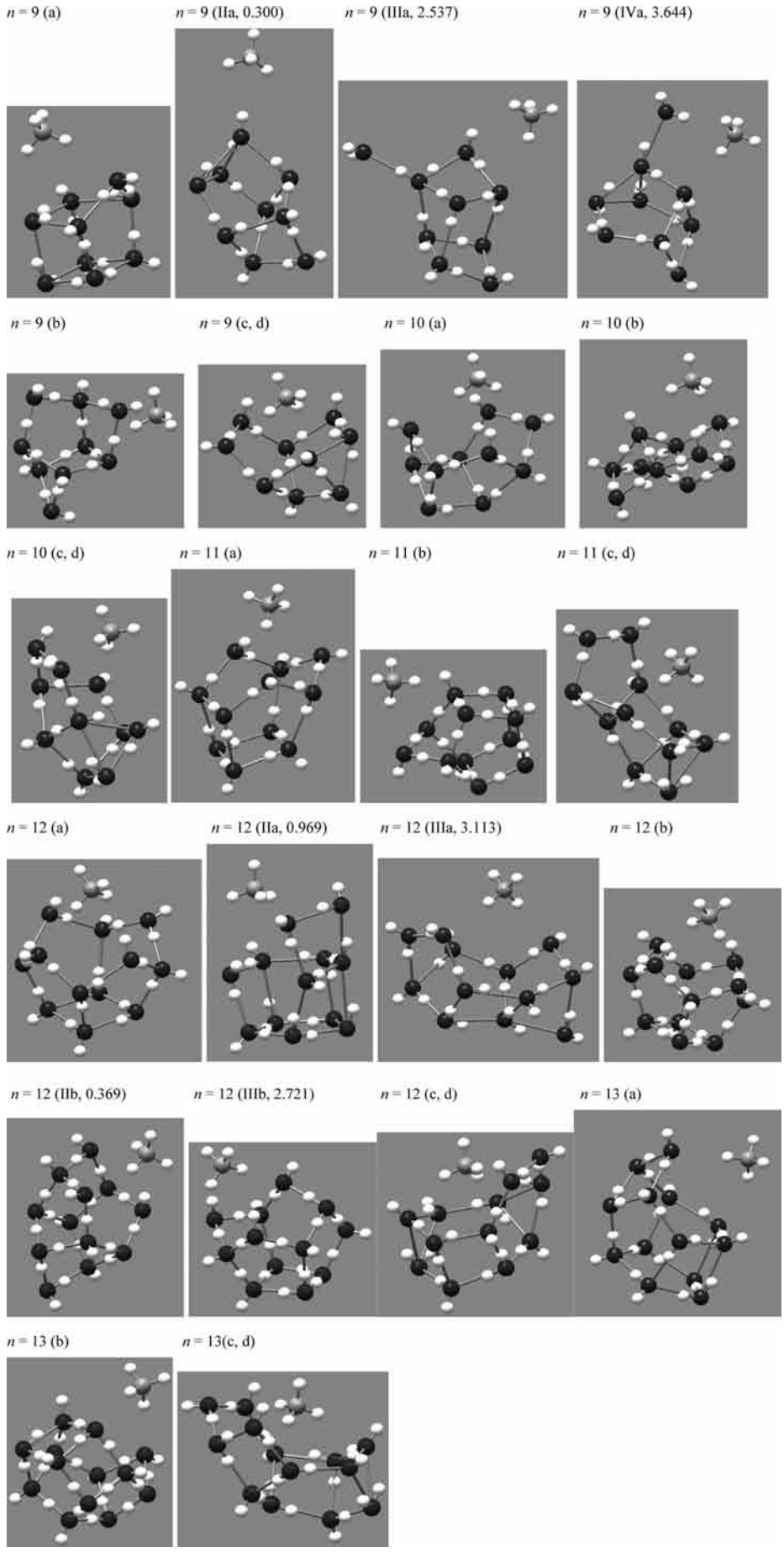

Figure 3. Geometry optimizations for the $n H_2O-CH_4$, $n = 9-13$, complex. The nomenclature is specified as in the footnote of Figure 1, and the geometry parameters are reported in Tables 5a (in the Supporting Information) and 5b.

TABLE 5B: Geometrical Parameters for the $CH_4-(9-13)H_2O$ Complex (Ångstroms, Degrees)

	MP2				B3LYP			
n	OO	OH	OHO	CO	OO	OH	OHO	CO
9	2.512	1.080	170.0	3.793	2.751	0.981	173.1	3.542
10	2.513	1.071	168.1	3.741	2.752	0.980	168.2	3.543
11	2.491	1.100	170.2	3.770	2.800	0.980	167.1	3.484
12	2.494	1.091	175.3	3.701	2.760	0.980	169.3	3.670
13	2.511	1.100	171	3.742	2.751	0.980	171.1	3.810

parameters were dramatically affected. The C−O curve showed at $n = n_e$ an abrupt shortening (of 20% for the MP2 method), which was a minimum for all methods. For larger *n* values the C−O distance started to be more relaxed. In any case, it tended to remain near the value at encapsulation. This could mean that the CH_4 molecule, once confined, remained so, also for larger sizes, as it seemed to occur, according to the obtained CH_4-nH_2O complex forms. At $n = 18$ the complex for all methods has the same number of subunits in its nH_2O cage, although the subunits were different. The smallest slopes occurred for the HF method, as was expected, because this behavior is heavily dictated by dispersive interactions.

For the O−O curve, all methods showed a contraction of the O−O distance for the $n = 2-4$ range. For $n > 4$ the O−O distance oscillated around a particular method-dependent value that is ∼2.50 Å for the MP2 method, ∼2.75 Å for the BH&H (B3LYP) method, and ∼2.90 Å for HF method. At $n = n_e$ all methods showed an increase in the O−O distance, that for larger sizes remained slightly relaxed relative to the distance before encapsulation. The MP2 method showed the smallest relaxation (∼5%). From the O−H distance drawn in Figure 6, the MP2 method denoted the most noticeable changes, with minima at $n = 6, 10, 12$, besides the minimum at $n = n_e$. The corresponding structures have the peculiarity of including a large number of square and pentagon subunits in their nH_2O forms. The other methods proved to be less sensitive. The OHO angle behavior is drawn in Figure 7. For the BH&H and B3LYP methods, starting at $n = 4$, it shows an increasing tendency that started to decrease at $n = 16$. After the CH_4 confinement, these methods showed two minima: at $n = 15$ and 20. For the HF and MP2 methods the tendencies were less noticeable, but for the latter region they showed also two minima, at $n = 18$ (HF, MP2) and $n = 20$ (MP2) and probably at $n = 21$ or larger for the HF method (from $n = 19$ the HF values decreased). In the region $n = 13-16$ the OHO averaged angle for all methods seemed to coincide, and the region at which it differs most is $n = 2-7$ and, in particular, the HF and MP2 values differ from the BH&H and B3LYP ones.

3.4. Frequency and Type of Subunit. Figures 8S−10S (in the Supporting Information) sample the type of subunits that comprise the nH_2O counterpart cluster in the CH_4-nH_2O complex and their frequency, that is, the number of times they repeat in it, considering only isomer I (except the $n = 16$ complex of the MP2 method, for which we considered the second isomer), although for the following analysis, all isomers reported in the earlier sections have been considered. From the figures it could be further confirmed that the square and pentagonal subunits are the most abundant for all sizes and methods. In particular, the HF and BH&H methods showed a larger number of squares (S) than pentagons (P), and the inverse situation occurred for the MP2 method. The S/P ratios for the HF, MP2, and BH&H (B3LYP) methods were as follows: 77/72, 47/76, and 72/54, respectively. These ratios are likely influenced by the additional number of isomers considered for each method (this number is included in Table 7). The HF and MP2 methods included more isomers than the BH&H (B3LYP) method. The frequency for the square subunit was confirmed not to be favored for the MP2 method, in contrast to the BH&H (B3LYP) method, which accounted for 72 squares that competed with 77 from the HF method, despite the fact that in the HF method eight isomers in addition isomer I were included and in the BH&H (B3LYP) method, only three. This confirms further that the BH&H (B3LYP) method favored compact forms, if compared with the other methods, and more remarkably for the $n = 14-21$ region (see the large frequency numbers at $n = 19$, 20, and 21). The hexa- and heptagon subunits became more apparent also for the large *n* range. These subunits started at $n = 7$, 8, and 9, respectively, for the HF, MP2, and BH&H (B3LYP) methods (Figures 8S−10S in the Supporting Information). The MP2 method accounted for the least compact forms. This method showed its largest population of small subunits in the $n = 9-13$ region. Counting the total number of subunits per method for the whole range, we obtained the following numbers, ordered from the triangle to the heptagon subunit (T/S/P/H/H): 5/77/72/16/9, 2/47/76/17/13, and 18/72/54/22/4, respectively, for the HF, MP2, and BH&H (B3LYP) methods. We stress the higher frequency of the triangular subunit in the BH&H (B3LYP) forms, found in earlier sections.

Finally, in Table 7 are reported the total numbers of subunits for each *n* region as well as their average value, considering the number of isomers in the region. The averaged values are also drawn in Figure 11S (in the Supporting Information). Looking at these behaviors, we could confirm tendencies discussed in the last paragraph, as for example, the preference of more compact forms for the MP2 method in the $n = 9-13$ region. Figure 11S includes a last region (4) that represents the total number of subunits for the whole range. Here, the MP2 method had the lowest number, influenced by the very low value reached in region 3. It seems then that the BH&H (B3LYP) method accounted for the most compact forms of the nH_2O clusters considering the whole $n = 1-21$ range.

3.5. Energy of Formation and Stability. The energy of formation of the CH_4-nH_2O complex per number of H_2O molecules can be analyzed with the following the equation:

$$E_b'/n = (E_{CH4} + nE_{H2O} - E_{cla})/n \quad (1)$$

Its behavior with *n* is shown in Figure 12. E_{cla} stands for the energy of the CH_4-nH_2O complex and E_{CH_4}, E_{H_2O} are energies of the CH_4 and H_2O molecules, respectively. For this and the next figure, isomer I was considered, with the exception of the $n = 16$ case for the MP2 method for which isomer II was taken instead. The curves in Figure 12 show a general increasing tendency with *n* that for the BH&H andB3LYP methods continued further for all of the range. For the HF and MP2 methods in the $n \geq n_e$ range, the behavior turned out to be approximately constant for the HF method and slightly decreasing for the MP2 method. The HF curve showed the lowest energies, as expected. For the $8 \rightarrow 9$, $12 \rightarrow 13$, and $15 \rightarrow 16$ steps, this curve showed very small gradients that could be associated with geometry transitions. Looking, for example, at the 8- and $9H_2O$ counterpart clusters, one could see a change from an open to a more compact structure. A similar situation could be explained for the $n = 12 \rightarrow 13$ transition. It goes from a structure of one square, four pentagons, and one octagon to one of four squares, three pentagons, and one heptagon. For the $n = 15 \rightarrow 16$ transition the complex goes from a structure of one triangle, two squares, three pentagons, and three hexagons to one of three squares, six pentagons, and one hexagon. The arrival at a more compact H_2O cluster could also be associated

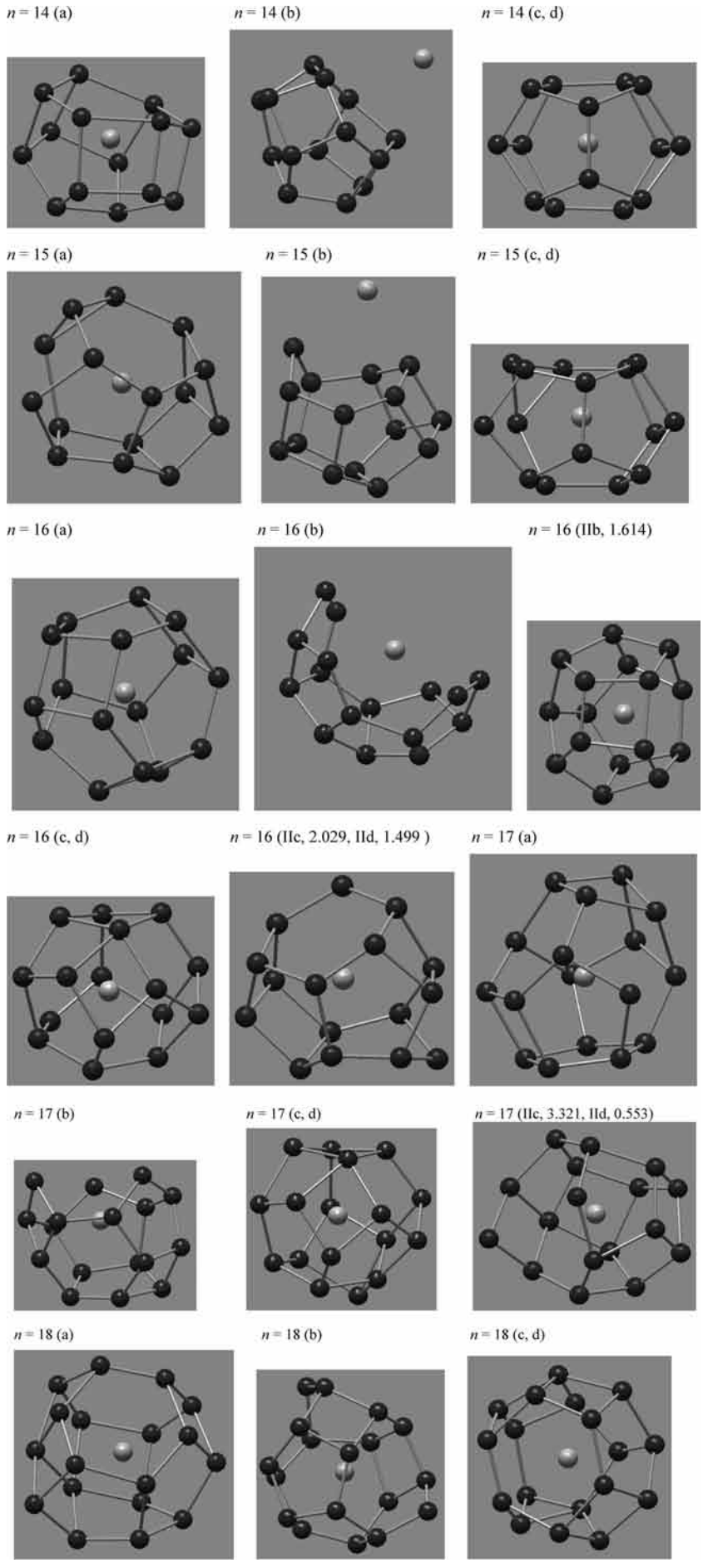

Figure 4. Part 1 of 2.

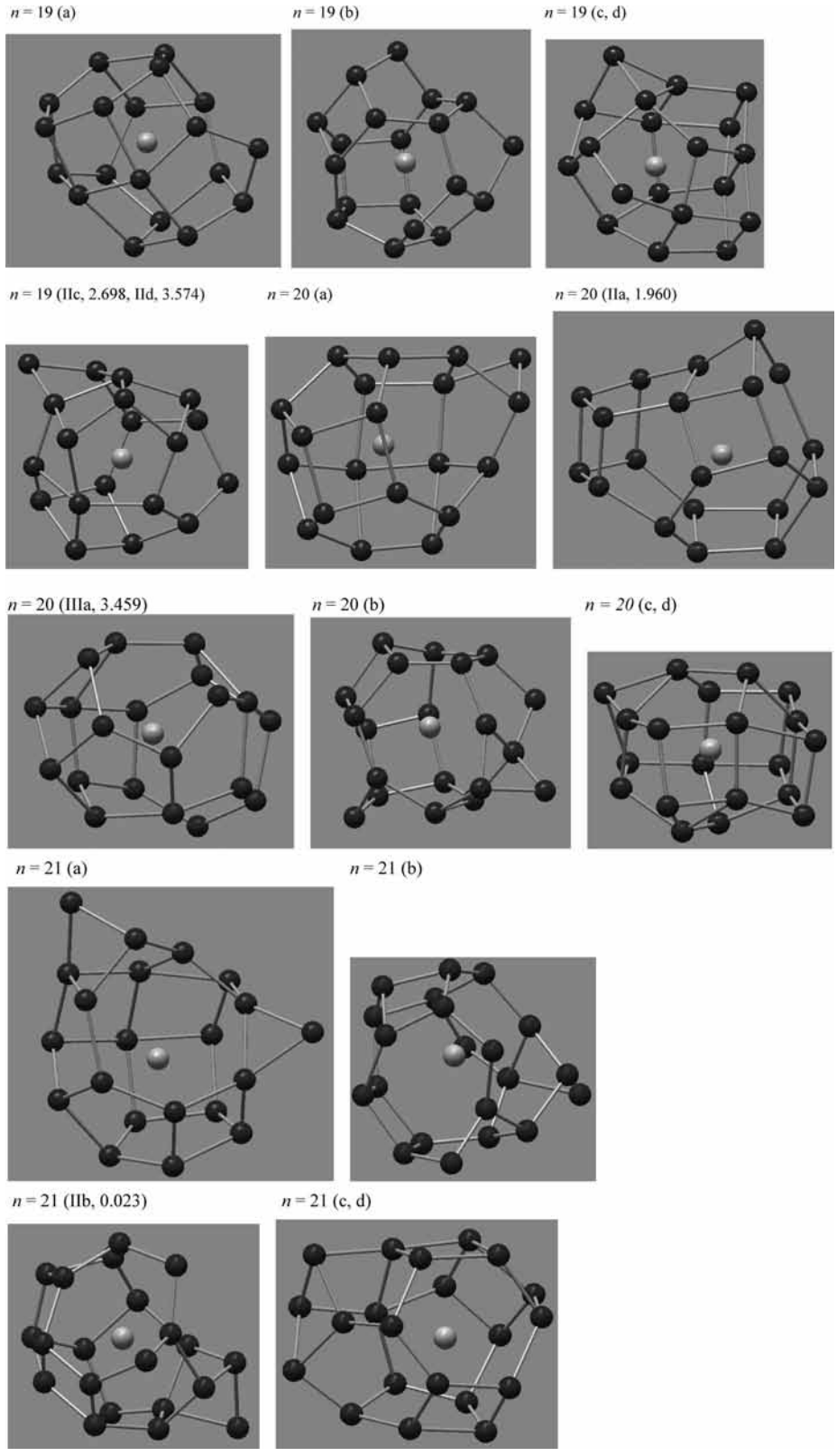

Figure 4b. Part 2 of 2. Optimized geometries for the nH_2O-CH_4, $n = 14-21$, complex. The nomenclature is explained in the caption of Figure 1, and geometry parameters are reported in Tables 6a (in the Supporting Information) and 6b.

with an increase in the number of H bonds. For these three transitions, this number increased by 3, in each case. This higher stability due to an increase in the number of H bonds is also in agreement with the literature of small water clusters and their isomers.[41]

For the other methods the curves showed a similar situation. A noticeable increase in the $n = 9 \rightarrow 10$ step of the BH&H (B3LYP) curve also agrees with an increase in the structure of the $10H_2O$ cluster, with the addition of a square subunit. For this same step the MP2 method showed a fall. At $n = 10$ the interaction of the CH_4 molecule with the $10H_2O$ cluster for this method showed a structure facing a 6-ring H_2O subunit that should not be the most favored approach. It may be noted that the complex normally shows a geometry in which the guest

TABLE 6B: Geometrical Parameters for the $CH_4-(14-21)H_2O$ Complex (Ångstroms, Degrees)

	MP2				B3LYP			
n	OO	OH	OHO	CO	OO	OH	OHO	CO
14	2.500	1.090	172.1	3.774	2.820	0.981	170.0	3.140
15	2.511	1.084	173.0	3.753	2.804	0.981	169.4	3.211
16[a]	2.552	1.073	173.0	2.990	2.771	0.981	171.0	3.252
17	2.500	1.110	175.2	3.030	2.790	0.981	170.0	3.301
18	2.511	1.090	174.3	3.160	2.802	0.981	169.3	3.392
19	2.513	1.091	175.2	3.041	2.782	0.982	169.2	3.283
20	2.511	1.090	171.0	3.081	2.840	0.981	166.4	3.200
21	2.511	1.090	172.0	3.232	2.781	0.982	169.3	3.202

[a] MP2 values correspond to isomer II.

molecule faces a square, pentagonal, or even a heptagonal subunit of the nH_2O cluster, but not necessarily a 6-ring form. The hexagonal ring form is not one of the most stable isomers of the $6H_2O$ cluster.[18,42,48] The $n = 10 \rightarrow 11$ transition for the MP2 method shows a large gradient that agrees with the preference of a pentagonal $5H_2O$ subunit facing the CH_4 in the $n = 11$ complex. This cluster accounts for an "almost cage" conformation, also with an averaged C−O distance shorter than at $n = 10$, providing, in this way, a more feasible interaction of the H_2O molecules with the CH_4 molecule.

The latter discussion suggests that the better stabilization for the CH_4-nH_2O complex should be related to the increase in the number of small subunits that form the nH_2O cluster. This was to be expected because the contribution of the nH_2O cluster to the stability of the complex has to be much larger than the contribution from the position of the guest molecule relative to it. The formation of an H bond in a water structure is about 1 order of magnitude larger than the London interaction of the guest molecule with the water network (this could be seen also with the comparison of D_e and ε values in Tables 1 and 4). But, interestingly, this fact is altered in the $13 \rightarrow 14$ step of the HF method, as well as in the $15 \rightarrow 16$ step of the MP2 method. For the HF curve, the $14H_2O$ structure is in fact formed with a larger number of small subunits (four squares, four pentagons, and one hexagon) than the $13H_2O$ structure (four squares, three pentagons, and one heptagon). Also at $n = 14$ occurs the first encapsulation of the CH_4 molecule, and the $E_b'/14$ value is here lower than at $n = 13$. It seems that for the HF and MP2 methods, the CH_4 molecule at encapsulation accounted for an energy contribution that lowered the binding energy of the complex. This situation for the MP2 curve is even more dramatic, with a fall at $n_e = 16$, of 0.64 kcal/mol. The BH&H and B3LYP curves behaved very similarly. Here, the $n = 13 \rightarrow 14$ transition did not result in a lowering of the binding energy, but in higher energies. Another difference relative to the HF and MP2 methods occurred at the $n = 20 \rightarrow 21$ step, with a slight energy increase, whereas with the HF and MP2 methods the energy decreased slightly.

To explain the increase or decrease in the binding energy at the CH_4 molecule encapsulation, we focused on a particular method-dependent property: the *confining volume* of the nH_2O cage. It depends on the O−O distance earlier discussed in Figure 5. The increase in the complex stability at the CH_4 molecule encapsulation seemed to depend on the size of the confining volume provided to the guest molecule, as well as on the electron correlation effect. The MP2 method produced the smallest cages. However, the BH&H and B3LYP methods produced middle-sized H_2O cages and included a reasonable description of the electron correlation effect, providing to the complex an enhancement in its stability at encapsulation.

Similar to eq 1, the energy of formation for the nH_2O counterpart cluster or cage that took part in the CH_4-nH_2O complex, per number of H_2O molecules, here defined as E_b/n, was estimated by using the following equation:

$$E_b/n = (nE_{H2O} - E_{clawg})/n \quad (2)$$

These energies are included in Figure 12. Strictly speaking, E_b/n is not the binding energy of the nH_2O cluster because its energy, E_{clawg} (labeling refers to the energy of the clathrate without guest), does not correspond to the optimized geometry of the nH_2O cluster, but to the geometry of the CH_4-nH_2O complex. The energy E_{clawg} came from a single-point calculation in the geometry of the CH_4-nH_2O complex without including the guest molecule. The interactions of the guest molecule with the H_2O network were assumed to be small, presumably, much smaller than the H bond energy that took part in the H_2O network, as we discussed in the paragraphs before. Therefore, the assumption that the geometry of the nH_2O cluster or cage was not expected to be straightforwardly different from its geometry in the CH_4-nH_2O complex, could be realistic.[49] With this assumption, slight differences were observed between the E_b/n and E_b'/n values. As expected, the HF energies behaved almost identically for the $n < n_e$ region. At $n = n_e$ a large gradient occurred and put $E_b > E_b'$. For larger sizes the energy gap remains, and $E_b > E_b'$. For the MP2 method a similar situation occurred. Here, the energy gap at $n = n_e$ was 0.879 kcal/mol and decreased for larger sizes, but is kept larger than at those sizes before encapsulation; furthermore, $E_b > E_b'$. Here, the character of the MP2 energy for $n > n_e$ changes, to be slightly decreasing.

The BH&H and B3LYP methods showed the most noticeable differences in the E_b and E_b' values for the $n = 1-3$ range and decreased monotonically with n. For the whole range, the B3LYP energies are slightly higher. For the $n = 1-13$ region the E_b' values were higher than E_b. At the $n = 13-14$ step an inversion is observed, caused by an enhanced increase in the $E_b/14$ value. This happens for both methods. For larger sizes, E_b and E_b' were close to each other, keeping $E_b < E_b'$ up to $n = 19$. At $n = 20$ a new inversion occurred, and at $n = 21$ the order was once more inverted ($E_b' > E_b$). The largest gradients in the E_b and E_b' values occurred in the $n = 1-4$ range for all methods. The values at $n = 3$ could help us understand the easier (energetically) way of forming triangular H_2O subunits with the BH&H and B3LYP methods, as was found in earlier sections.

The MP2, BH&H, and B3LYP methods accounted for a very good description of the electron correlation effect, but its interplay with the size of the available volume provided by the H_2O cage to confine the CH_4 molecule seems to be, as well, important to determine the stability of the CH_4-nH_2O complex.

Substracting eq 2 from eq 1, the following equation

$$E_b - E_b' = E_{cla} - E_{clawg} - E_{CH4}, \text{ for } n = 1, ..., 21 \quad (3)$$

is obtained, and its behavior with n has been drawn in Figure 13. Written in this way, eq 3 could help us better visualize the CH_4 molecule interaction with the nH_2O counterpart structure. For the $n < n_e$ range, $E_b - E_b'$ is negative for all methods. For the HF and MP2 methods, the energies are close to each other and close to 0, whereas the BH&H and B3LYP methods show even closer values between each other and values further from 0. A very small $E_b - E_b'$ value means that the guest molecule is almost unaffected by the presence of the nH_2O cluster or is at most very poorly attracted. Up to $n = 4$ the tendency coincided for the four methods. For $n > 4$ more noticeable

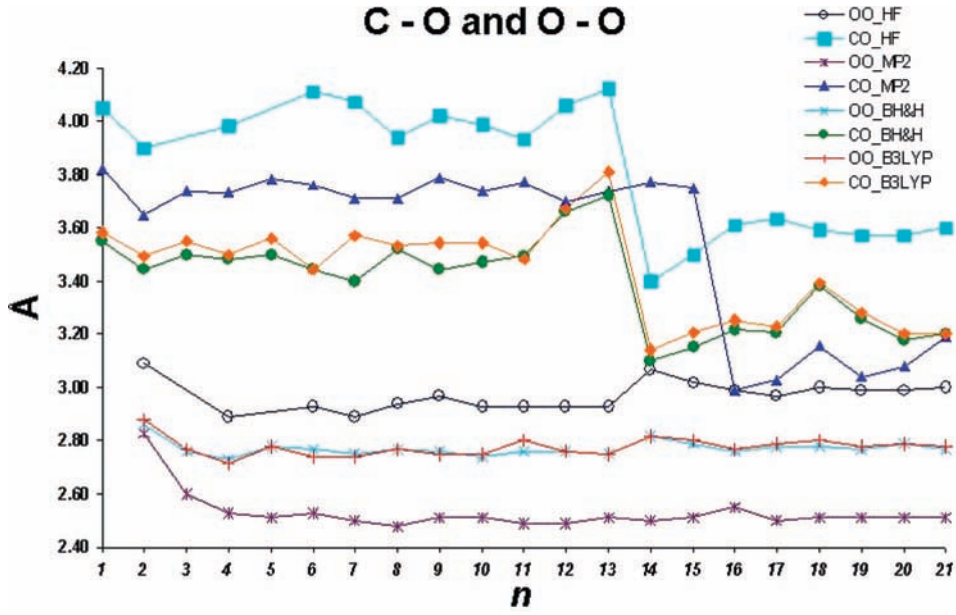

Figure 5. C−O and O−O parameter distance as a function of n.

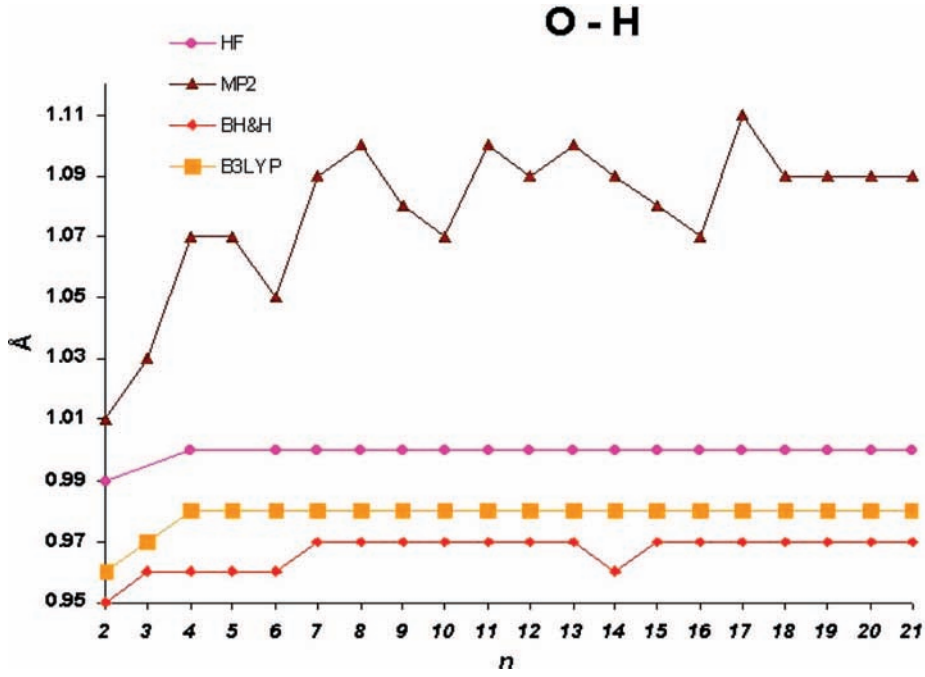

Figure 6. O−H distance as a function of n.

changes were observed between the HF and MP2 methods and the BH&H and B3LYP methods, as can be seen in the n = 9−13 range, where the former group of methods (HF, MP2) showed in each step slopes that were sign-inverted from the latter group. Noticeable minima occurred at n = 12 for the HF and MP2 methods and at n = 2 and 13 for the BH&H and B3LYP methods. With the HF and MP2 methods, the geometry transitions from n = 11 to n = 13 showed a ring or kind of ring subunit facing the CH_4 molecule, which went from 7 and 5 sizes, respectively, for HF and MP2 methods, at n = 11, to 8 and 8, at n = 12, and then to 7 and 7, at n = 13. The $12H_2O$ cluster had the largest ring and showed the strongest $CH_4 \leftrightarrow nH_2O$ attraction. For the BH&H and B3LYP methods at the $n = 12 \rightarrow 13$ step a similar situation occurred, that is, the water structure went from an 8-ring subunit at n = 12 to a nonagon ring at n = 13, to face the CH_4 molecule. For the minimum at n = 2, the same behavior applies: The noticeable increase in the correlation effect for the $3H_2O$ cluster contracted the O−O distance, reducing consequently the size of the (triangular) ring with which the CH_4 molecule could interact. Therefore, also the C−O distance comes out to be larger than at the n = 2 complex. It seems then that before the CH_4 molecule confinement, the complex showing the larger subunit area that faces the CH_4 molecule is a good candidate to have a large attractive interaction with it.

The $E_b - E_b'$ behavior for larger sizes ($n \geq n_e$) included the first CH_4 molecule confinement that is easily identified with the very large (positive) slope at $n = n_e$, and it happens so for all methods, turning the $E_b - E_b'$ negative gap into positive. This means then that the CH_4 molecule, once confined, contributes with a repulsive interaction to the water cage. For $n > n_e$, the HF and MP2 methods remained with positive energies. The HF curve had a monotonic decrease that started from its maximum at $n = n_e$, and the MP2 curve showed a

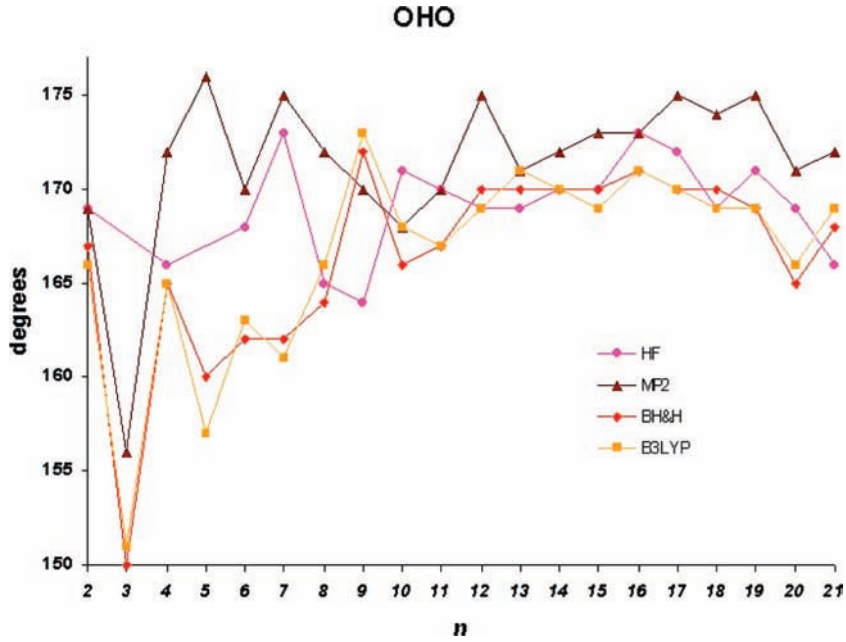

Figure 7. OHO angle as a function of *n*.

TABLE 7: Total Number of Subunits per *n* Range or Region (See also Figure 11S)

region	*n*	HF	HF_av[a]	MP2	MP2_av	BH&H (B3LYP)	BH_av
1	2−8	12 (1)[b]	1.5	17 (2)	1.7	16	2.3
2	9−13	62 (5)	6.2	46 (2)	6.6	32	6.4
3	14−21	113 (2)	11.3	96 (2)	9.6	127 (3)	11.6
4[c]	total	187 (8)	19	159 (6)	18	175 (3)	20.3

[a] Number of subunits in the region, divided by the total number of isomers in the region. [b] Number in parentheses is the number of isomers in addition to I, in the region. [c] Values are obtained as $\text{region}_4 = \Sigma_i = 1-3\ \text{region}_i$.

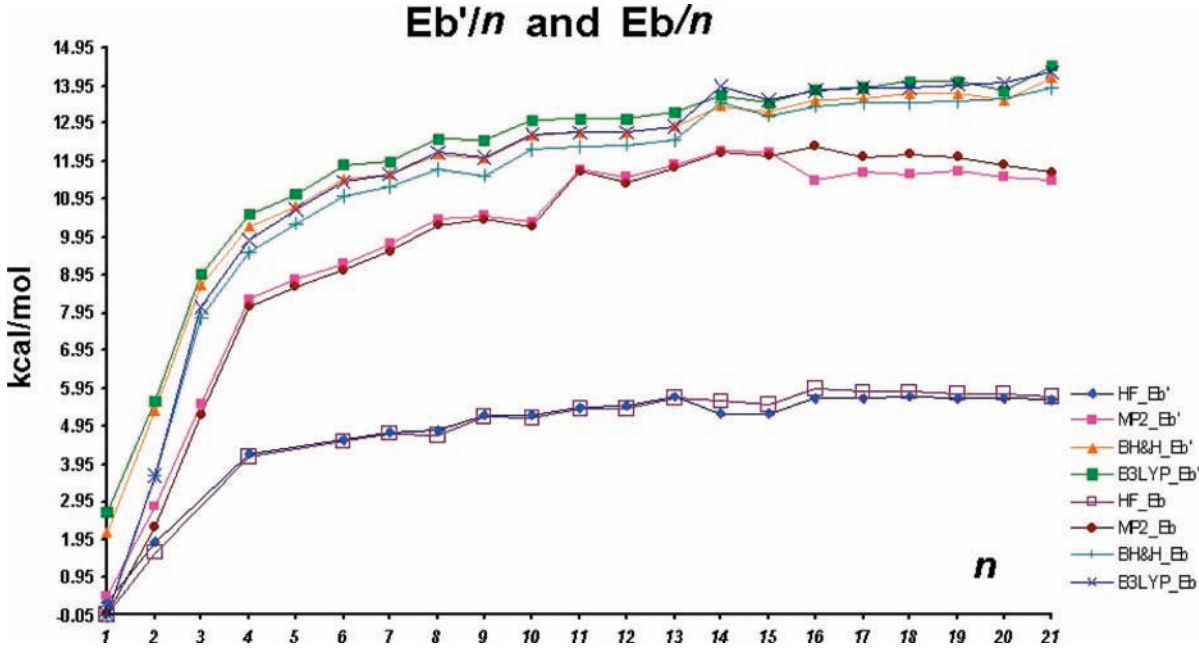

Figure 12. Binding energy E_b'/n and E_b/n versus *n*, defined respectively in eqs 1 and 2.

stepwise behavior that was not so clear in the $n < n_e$ region. For this method, the energy at $n = n_e$ represented the highest peak, also among methods. The responsible complex of this energy has a $16H_2O$ cage with a high number of very small subunits (also understood as a high structure) that included as its largest subunit a hexagonal ring (see Figure 4). Its neighbors, at $n = 15$ and 17, reported lower $E_b - E_b'$ values that accordingly included in their water cages, respectively, the heptagon and the nonagon rings, which are larger subunits.

For the BH&H and B3LYP methods, the energy gap changed after $n = n_e$ to negative values up to $n = 19$ (except for the value at $n = 15$ in the B3LYP curve), and both methods behaved qualitatively the same. At $n = 20$ both curves showed a very large slope that is also related to the high structure of the $20H_2O$

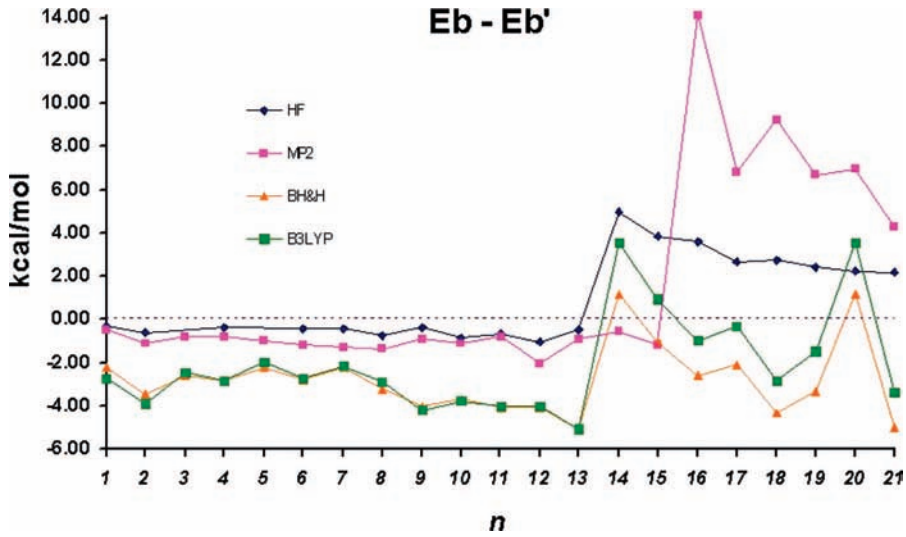

Figure 13. $E_b - E_b'$ versus n. See eq 3 in the text.

trapping cage. It is composed by two triangles, eight squares, and six pentagonal subunits; and by comparison with its neighbors, at $n = 19$ and 21, where the structures present a heptagon and three hexagons, respectively, as the largest subunit, the $20H_2O$ has higher structure. The more compact is the nH_2O cage hosting the guest molecule, the larger is the repulsive effect. As the $21H_2O$ cage is less compact than the $19H_2O$ cage, the energy at $n = 21$ is lower than at $n = 19$. The CH_4 molecule at confinement seems to provide, in fact, a repulsive contribution to the complex.

3.6. Classical Interpretation. In this section we present a simple classical picture of the observed behavior after the CH_4 molecule encapsulation, that is, for $n \geq n_e$. Figure 13 shows a maximum in the energy gap at $n = n_e$, which means that the CH_4 molecule contributes a repulsive interaction to the water cage. Given that for this n value, the smallest C−O distance within the complex shows a minimum (see Figure 5), it is intuitive that the CH_4 molecule will add a large repulsive term to the total Hamiltonian, because for small C−O distances, the $CH_4 \leftrightarrow H_2O$ pair interaction is mainly repulsive, as shown in Figure 2S (Supporting Information). Therefore, also, the energy gap tendency is to decrease for larger sizes, $n > n_e$, because then the cages are larger and the water network is farther from the CH_4 molecule.

The contribution of the CH_4 molecule to the total energy of the clathrate can be understood by using a simple picture of the interaction between polar and nonpolar molecules. We assume that the CH_4 molecule behaves as a non polar molecule (its dipole moment is at least 3 orders of magnitude less than that of a H_2O molecule). If we calculate the pair interaction between a polar and a nonpolar molecule, like the one shown in Figure 2S (Supporting Information), the only way these two molecules can interact is through a soft-sphere type potential, because in principle any relative orientation between them will not change the energy at a fixed distance, because dipole−dipole and higher order electrostatic interactions are negligible. Therefore, all that happens between these two molecules can be explained by their size, σ, and the well depth, ε.

It is easy to see that for small H_2O cages, as the ones obtained with the MP2 method, the $E_b - E_b'$ values are the most repulsive because there is an available confining volume that is too tight for the CH_4 molecule (the water cage diameter is probably less than the CH_4 molecule diameter, σ_{CH4}). When the CH_4 molecule is confined, the presence of big holes or big ring subunits ($n > n_e$) also increases the available space within the water cage, providing more room for the CH_4 molecule, which contributes a less repulsive term to the complex energy.

From Figure 2S (Supporting Information), it is straightforward to obtain an approximate value for the size (diameter) of the CH_4 molecule. Strictly speaking, the value of σ, where the $CH_4 \leftrightarrow H_2O$ potential becomes 0 in Figure 2S, is given by

$$\sigma = (\sigma_{H2O} + \sigma_{CH4}))/2 \quad (4)$$

according to the Lorentz−Berthelot mixing rules.[50] By comparing directly the σ values of the HF and MP2 methods with the C−O distances of Tables 3−5, the latter distances are shorter than σ for all $n \geq n_e$, which explains in a simple way the repulsive $CH_4 \leftrightarrow nH_2O$ interaction. For the other two methods, the averaged interaction of the CH_4 molecule with the water network showed not to be representative from the C−O minimum complex distance that we reported in the tables. In these methods, we conclude that electrostatic interactions and therefore the relative orientation between the molecules are not negligible as to treat them only as soft spheres; nevertheless, the σ values in this case will still give us a very good idea of the qualitative behavior of the interactions and stability.

Let us remember that the relative orientation between the CH_4 and H_2O molecules in which we started the optimization of the $n = 1$ complex came from the $n = 2$ complex. Then, for any nH_2O cage that was composed as a combination of several $(n - x)H_2O$ subunits, the relative orientation between each H_2O molecule and the CH_4 molecule should be different. A starting C−O optimization for CH_4-H_2O pair molecules, taken from every water orientation of the optimized geometry in the CH_4-nH_2O complex, would be probably a better approach to obtain a σ value as a threshold for attractive and repulsive energies between the guest molecule and the water network in the CH_4-nH_2O complex.

Despite our results being apparently opposite from the common belief that CH_4-nH_2O complexes with lowest energies are the most stable ones, it has been argued by P. M. Rodger that mechanical stability may be enhanced by repulsive interactions of the CH_4 molecule with the water cage.[51]

Conclusions

Molecular calculations using the HF/cep-4 g, MP2/cep-4 g methods, including d and p polarization functions, respectively,

to O and H atoms, as well as the BHandHLYP/6-311 g(d,p), and B3LYP/6-311 g(d,p) methods, were carried out to study the CH_4-nH_2O complex, for $n = 1-21$. A good description of the H bond in the modeling of a H_2O cluster, H_2O cage, or in general any H_2O network is crucial to observe tetrahedral ordering. As well, the guest ↔ host interaction, which may be of at least 1 order of magnitude smaller than the energy of an H bond in the water network, has to be reproducible.

Although some differences among methods were apparent, overall the methodologies we used described the $CH_4 \leftrightarrow nH_2O$ interaction properly, as well as the H bond in the formation of the water structures.

From our results, we could extract the basic physics of the $E_b - E_b'$ behavior as a function of n, as well as of the nH_2O structure, the parameters of which agreed well with the water clusters reported in the literature. We also showed that the guest ↔ host interactions can be described mainly by soft-sphere type potentials (soft repulsion and induced dipole ↔ dipole interactions).

Furthermore, we identified method-independent features. One of them is the presence of square and pentagonal subunits for the very small sizes that became characteristic also for the rest of the n series. Another feature is the abrupt change in some of the geometry parameters at the CH_4 molecule encapsulation, as were the C–O and O–O distances (Figure 5). Or from the energetic point of view, the E_b-E_b' versus n curve (Figure 13), showing a completely different character before and after encapsulation, is also a feature. At $n = n_e$, with the largest maximum of this curve, came out to be the most remarkable and apparently contradictory feature to hydrate stability. We concluded that this maximum at encapsulation is mainly due to a soft repulsion between the CH_4 molecule and the water cage, and the observed decreasing behavior in the energy gap for $n > n_e$ for the HF and MP2 methods is easily understood in terms of the available space within the water cage that hosts the CH_4 molecule, being larger as n increased. The presence of the CH_4 molecule in the water cage requires a volume that may be larger than the volume availability provided by the water cage, so that a soft repulsion from the $CH_4 \leftrightarrow nH_2O$ interaction accounts for a positive contribution to the $E_b - E_b'$ gap. However, this repulsion may not be enough to break any of the H bonds of the water network, and therefore the CH_4 molecule remains confined.

We argued that for the BH&H and the B3LYP methods, the $CH_4 \leftrightarrow nH_2O$ interaction is mainly dominated by a soft-sphere term, so we can describe qualitatively the observed behavior of the energy gap by using the same physical arguments. We finally assumed that in these two methods, permanent dipole ↔ dipole and higher order electrostatic interactions may be relevant if one would like to explain exactly the observed behavior that could offer a nice numeric match for future useful investigations on classical simulation of hydrates.

Acknowledgment. This work was developed under Research Projects D.00345 and D.00406 of the Molecular Engineering Research Program of Instituto Mexicano del Petróleo (IMP). We thank the Supercomputing Laboratory of IMP for supercomputer time facilities. G.B.-P. thanks Prof. Jullius Jellinek for insightful comments at the beginning of this work and Dr. Ernesto Hernández Cooper, with whom, through his one-year postdoctoral position stay at IMP, valuable discussions were established for the interpretation of these results, as well as the referees for comments that contributed to the enrichment of the manuscript.

Supporting Information Available: Additional tables and figures. This information is available free of charge via the Internet at http://pubs.acs.org.

References and Notes

(1) Stern, L. A.; Kirby, S. H.; Durham, W. B. *Science* **1996**, *273*, 1843.
(2) Hallstein Fadnes, F. N. *Fluid Phase Equilib.* **1996**, *117*, 186.
(3) Mehta, A. P.; Sloan, E. D., Jr. *J. Chem. Eng. Data* **1994**, *39*, 887.
(4) Gaillard, C.; Monfort, J. P.; Peytavy, J. L. *Oil Gas Sci. Technol.—Rev. IFP* **1999**, *54* (3), 365.
(5) Sloan, E. D. *Am. Mineral.* **2004**, *89*, 1155.
(6) Subramanian, S.; Ballard, A. L.; Kini, R. A.; Dec, S. F.; Sloan, E. D., Jr. *Chem. Eng. Sci.* **2000**, *55*, 5763.
(7) Fujioka, T.; Jyosui, K.; Nishimura, H.; Tei, K. *Jpn. J. Appl. Phys.* **2003**, *42*, 5648.
(8) Holder, G. D.; Stephenson, J. L.; Joyce, J. J.; John, V. T.; Kamath, V. A.; Malekar, S. *Ind. Eng. Chem. Process Des. Dev.* **1983**, *22*, 170.
(9) Zhang, S. X.; Chen, G. J.; Ma, C. F.; Yand, L. Y.; Guo, T. M. *J. Chem. Eng. Data* **2000**, *45*, 908.
(10) Maekawa, T. *J. Chem. Eng. Data* **2003**, *48*, 1283.
(11) Riestenberg, D.; West, O.; Lee, S.; McCallum, S.; Phelps, T. J. *Mar. Geol.* **2003**, *198*, 181.
(12) Zhang, Y. *Geophys. Res. Lett.* **2003**, *30* (7), 1398.
(13) Guggenheim, S.; Koster van Groos, A. F. *Geology* **2003**, *31*, 7653.
(14) Quocle, H. An experimental study of CO_2 hydrate formation and dissociation. Master's of Science Thesis, School of Petroleum and Geological Engineering, Norman, OK, 2002.
(15) Circone, S.; Stern, L. A.; Kirby, S. H.; Durham, W. B.; Chakoumakos, B. C.; Rawn, C. J.; Rondinone, A. J.; Ishii, Y. *J. Phys. Chem. B* **2003**, *107*, 5529.
(16) (a) Sloan, E. D. *Clathrate Hydrates of Natural Gases*; Dekker: New York, 1990. (b) Sloan, E. D. *Energy Fuels* **1998**, *12*, 191.
(17) Stevens, W.; Basch, H.; Krauss, J. *J. Chem. Phys.* **1984**, *81*, 6026.
(18) Keutch, F. N.; Saykally, R. J. *Proc. Natl. Acad. Ssci. U.S.A.* **2001**, *98* (19), 10533.
(19) Dyke, T. R.; Muenter, J. S. *J. Chem. Phys.* **1974**, *60*, 2929.
(20) Curtiss, L. A.; Frurip, D. J.; Blander, M. *J. Chem. Phys.* **1979**, *71*, 2703.
(21) Markham, G. D.; Glusker, J. P.; Bock, C. W. *J. Phys. Chem. B* **2002**, *106*, 5118.
(22) Zhan, C.-G.; Dixon, D. A. *J. Phys. Chem. B* **2003**, *107*, 4403.
(23) Ruckenstein, E. R.; Shulgin, I. L.; Tilson, J. L. *J. Phys. Chem. A* **2003**, *107*, 2289.
(24) Zhan, C.-G.; Dixon, D. A. *J. Phys. Chem. A* **2004**, *108*, 2020.
(25) Alvarez-Idaboy, J. R.; Galano, A.; Bravo-Pérez, G.; Ruíz, M. E. *J. Am. Chem. Soc.* **2001**, *123*, 8387.
(26) Bravo-Pérez, G.; Alvarez-Idaboy, J. R.; Cruz-Torres, A.; Ruíz, M. E. *J. Phys. Chem. A* **2002**, *106*, 4645.
(27) Bravo-Pérez, G.; Alvarez-Idaboy, J. R.; Galano, A.; Cruz-Torres, A. *Chem. Phys.* **2005**, *310* (1−3), 213.
(28) Odutola, J. A.; Dyke Partially, T. R. *J. Chem. Phys.* **1980**, *72*, 5062.
(29) Yu, H.; van Gunsteren, W. F. *J. Chem. Phys.* **2004**, *121*, 9549.
(30) http://online.uis.edu/spring2000/che367/m1-geometry/sld005.htm.
(31) (a) http://www.lsbu.ac.uk/water/hbond.html. Hasted, J. B. Liquid water: dielectric properties. In *Water: A Comprehensive Treatise*; Franks, F., Ed.; Plenum Press: New York, 1972; Vol. 1, pp 255−309. (b) Silvestrelli, P. L.; Parrinello, M. *J. Chem. Phys.* **1999**, *111*, 3572.
(32) Wales, D. J. In *Encycopedia of Computational Chemistry*; Schleyer, P. v. R., Allinger, N. L., Clark, T., Gasteiger, J., Schaefer, P. A., III, Schreiner, P. R., Eds.; Wiley: New York, 1998; Vol. 5, p 3183.
(33) Frisch, M. J.; Trucks, G. W.; Schlegel, H. B.; Scuseria, G. E.; Robb, M. A.; Cheeseman, J. R.; Zakrzewski, V. G.; Montgomery, J. A., Jr.; Stratmann, R. E.; Burant, J. C.; Dapprich, S.; Millam, J. M.; Daniels, A. D.; Kudin, K. N.; Strain, M. C.; Farkas, O.; Tomasi, J.; Barone, V.; Cossi, M.; Cammi, R.; Mennucci, B.; Pomelli, C.; Adamo, C.; Clifford, S.; Ochterski, J.; Petersson, G. A.; Ayala, P. Y.; Cui, Q.; Morokuma, K.; Malick, D. K.; Rabuck, A. D.; Raghavachari, K.; Foresman, J. B.; Cioslowski, J.; Ortiz, J. V.; Stefanov, B. B.; Liu, G.; Liashenko, A.; Piskorz, P.; Komaromi, I.; Gomperts, R.; Martin, R. L.; Fox, D. J.; Keith, T.; Al-Laham, M. A.; Peng, C. Y.; Nanayakkara, A.; Gonzalez, C.; Challacombe, M.; Gill, P. M. W.; Johnson, B.; Chen, W.; Wong, M. W.; Andres, J. L.; Head-Gordon, M.; Replogle, E. S.; Pople, J. A. *Gaussian 98, Revision A.3*; Gaussian, Inc.: Pittsburgh, PA, 1998.
(34) Hollenstein, H.; Marquardt, R. R.; Quack, M.; Suhm, M. A. *J. Chem. Phys.* **1994**, *101* (5), 3588.
(35) Xantheas, S. S.; Dunning, T. H. *J. Chem. Phys.* **1993**, *98* (10), 8037.
(36) Dykstra, C. E. *Chem. Phys. Lett.* **1999**, *299*, 132.
(37) Xantheas, S. S. *J. Chem. Phys.* **1995**, *102* (11), 4505.
(38) Xantheas, S. S. *J. Chem. Phys.* **1994**, *100* (10), 7523.

(39) Cruzan, J. D.; Broten; M, G.; Liu, K.; Braly, L. B.; Saykally, R. J. *J. Chem. Phys.* **1996**, *105* (16), 6634.
(40) Batista, E. R.; Xantheas, S. S.; Jonsson, H. *J. Chem. Phys.* **1999**, *111* (13), 6011.
(41) Xantheas, S. S.; Burnham, C. J.; Harrison, R. J. *J. Chem. Phys.* **2002**, *116* (4), 1493.
(42) Burnham, C. J.; Xantheas, S. S.; Miller, M. A.; Applegate, B. E.; Miller, R. E. *J. Chem. Phys.* **2002**, *117* (3), 1109.
(43) Dunn, M. E.; Pokon, E. K.; Shields, G. C. *J. Am. Chem. Soc.* **2004**, *126*, 2647.
(44) Day, M. B.; Kirschner, K. N.; Shields, G. C. *J. Phys. Chem. A* **2005**, *109*, 6773.
(45) Xantheas, S. S.; Apra, E. *J. Chem. Phys.* **2004**, *120* (2), 823.
(46) Wales, J. D.; Hodges, M. P. *Chem. Phys. Lett.* **1998**, *286*, 65.
(47) Kirschner, K. N.; Hartt, G. M.; Evans, T. M.; Shields, G. C. *J. Chem. Phys.* **2007**, *126* (15), 154320.
(48) Maheshwary, S. H.; Patel, N.; Sathyamurthy, N.; Kulkarni, A. D.; Gadre, S. R. *J. Phys. Chem. A* **2001**, *105*, 10525.
(49) See the site Hydrophobic Hydration in http://www.lsbu.ac.uk/water/phobic.html, and references therein.
(50) Hirschfelder, J. O.; Curtiss, C. F.; Bird, R. B. *Molecular Theory of Gases and Liquids*; Wiley: London, U.K., 1954.
(51) Rodger, P. M. *Mol. Simulation* **1990**, *5*, 315.
(52) Petrenko, V. F.; Whitworth, R. W. *Physics of Ice*; Oxford University Press: Oxford, U.K., 1999.
(53) Fanourgakis, G. S.; Xantheas, S. S. *J. Chem. Phys.* **2006**, *124*, 174504(−1)
(54) Batista, E. R.; Xantheas, S. S.; Jonsson, H. *J. Chem. Phys.* **1998**, *109*, 4546.
(55) Huisken, F.; Kaloudis, M.; Kulcke, A.; Voelkel, D. *Infrared Phys. Technol.* **1995**, *36*, 171.
(56) Maheshwary, S. H.; Patel, N.; Sathyamurthy, N.; Kulkarni, A. D.; Gadre, S. R. *J. Phys. Chem. A* **2001**, *105*, 10525.
(57) Blanksby, S. J.; Ellison, G. B. *Acc. Chem. Res.* **2003**, *36*, 255.

JP7106268